Supporting Information

Synthesis and RAFT polymerisation of hydrophobic acrylamide monomers derived from plant oils

Oliver J. Harris, [a] Peter Tollington, [b] Calum J. Greenhalgh, [c] Ryan R. Larder, [a] Helen Willcock, [a] and Fiona L. Hatton *[a]

[a] Department of Materials, Loughborough University, Loughborough, LE11 3TU, UK.

[b] Cargill, Evert van de Beekstraat 378, 1118 CZ Schiphol, The Netherlands.

[c] Department of Chemistry, Loughborough University, Loughborough, LE11 3TU, UK.

*Corresponding author email: f.hatton@lboro.ac.uk

^{1}H NMR analyses of plant oils, kinetic evaluations of plant oil based monomer syntheses (OVM, HCM, HRM), transesterification side reaction study, characterisation of column purified HO-Sun monomer; ^{13}C NMR and DEPT-135, FTIR and LC-MS, ^{1}H NMR analysis of brine washed OVM, HCM, HRM, yield, purity and melting points for HOSM, OVM, HCM, HRM isolated by brine washing, GPC, TGA results and ^{1}H NMR for purified free radical polymers, initial RAFT CTA screening, kinetic evaluations for the RAFT polymerisations of brine washed OVM and HRM, conversion during RAFT polymerisations of HCM doped with HO-Sun, GPC chromatogram of kinetics samples of the RAFT polymerisation of HCM showing evidence of RAFT pre-equilibrium species formation, and demonstrating RAFT chain end fidelity, second RAFT screening results, TGA and DSC characterisations of plant oil based polymers and ^{1}H NMR spectra for py-CTA and end group analysis.

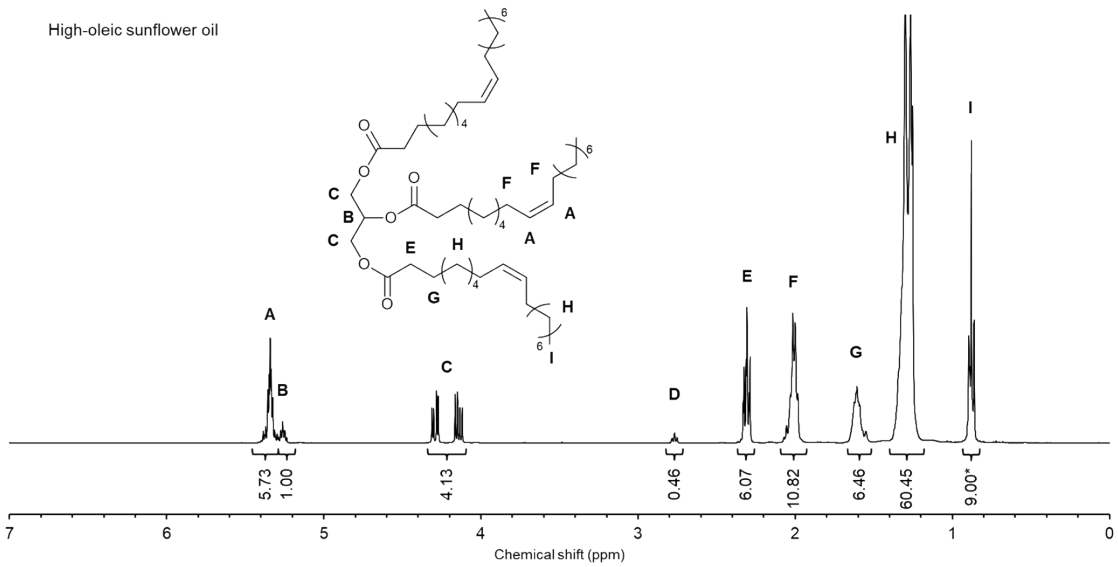

Figure S1. ^{1}H NMR spectrum (400 MHz, $CDCl_3$, 25 °C) of high-oleic sunflower oil. Peaks have been assigned to the target structure and integrals (referenced against the CH_3 signal at 0.89 ppm) are displayed.
^{1}H NMR (400 MHz; $CDCl_3$) δ_H (ppm): 5.36 (6H, m, -CH_2C**H**=C**H**CH_2-, mono-unsaturated FA), 5.26 (1H, m, -O-CH_2-C**H**O-CH_2-O-), 4.18 (4H, m, -O-C**H**$_2$-CHO-C**H**$_2$-O-), 2.77 (m, =HC-C**H**$_2$-CH=, poly-unsaturated FA), 2.33 (6H, t, -OCO-C**H**$_2$-), 2.03 (12H, m, -C**H**$_2$-CH=CH-C**H**$_2$-, mono-unsaturated FA), 1.59 (6H, m, -OCO-CH_2C**H**$_2$-), 1.28 (60H, m, -(C**H**$_2$)$_n$-), 0.89 (6H, t, -C**H**$_3$).

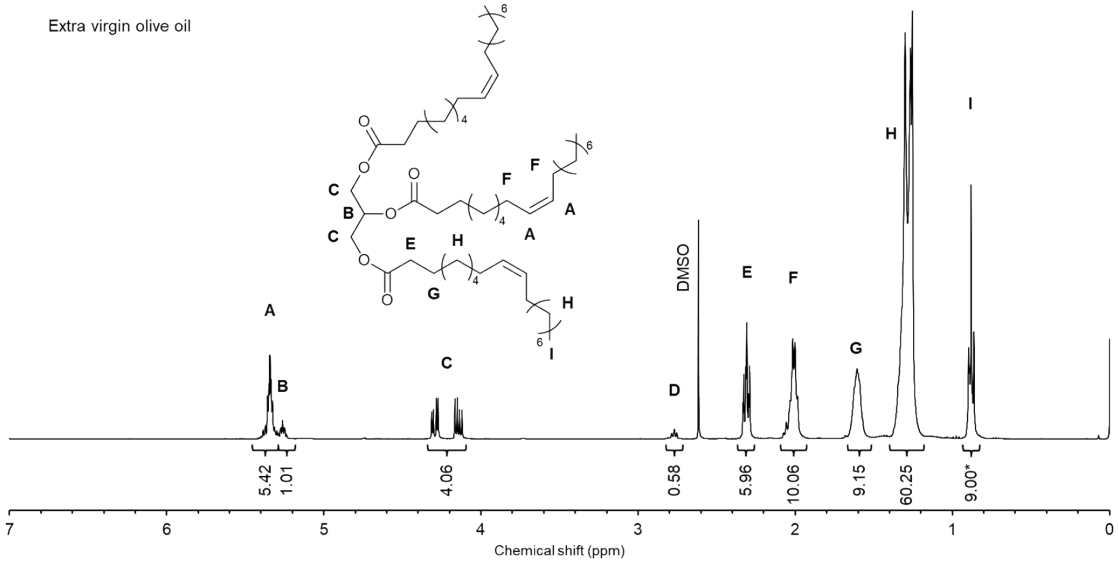

Figure S2. ^{1}H NMR spectrum (400 MHz, $CDCl_3$, 25 °C) of extra virgin olive oil. Peaks have been assigned to the target structure and integrals (referenced against the CH_3 signal at 0.88 ppm) are displayed.
^{1}H NMR (400 MHz; $CDCl_3$) δ_H (ppm): 5.35 (6H, m, -CH_2C**H**=C**H**CH_2-, mono-unsaturated FA), 5.26 (1H, m, -O-CH_2-C**H**O-CH_2-O-), 4.20 (4H, m, -O-C**H**$_2$-CHO-C**H**$_2$-O-), 2.79 (m, =HC-C**H**$_2$-CH=, poly-unsaturated FA), 2.32 (6H, t, -OCO-C**H**$_2$-), 2.03 (12H, m, -C**H**$_2$-CH=CH-C**H**$_2$-, mono-unsaturated FA), 1.64 (6H, m, -OCO-CH_2C**H**$_2$-), 1.32 (60H, m, -(C**H**$_2$)$_n$-), 0.88 (6H, t, -C**H**$_3$).

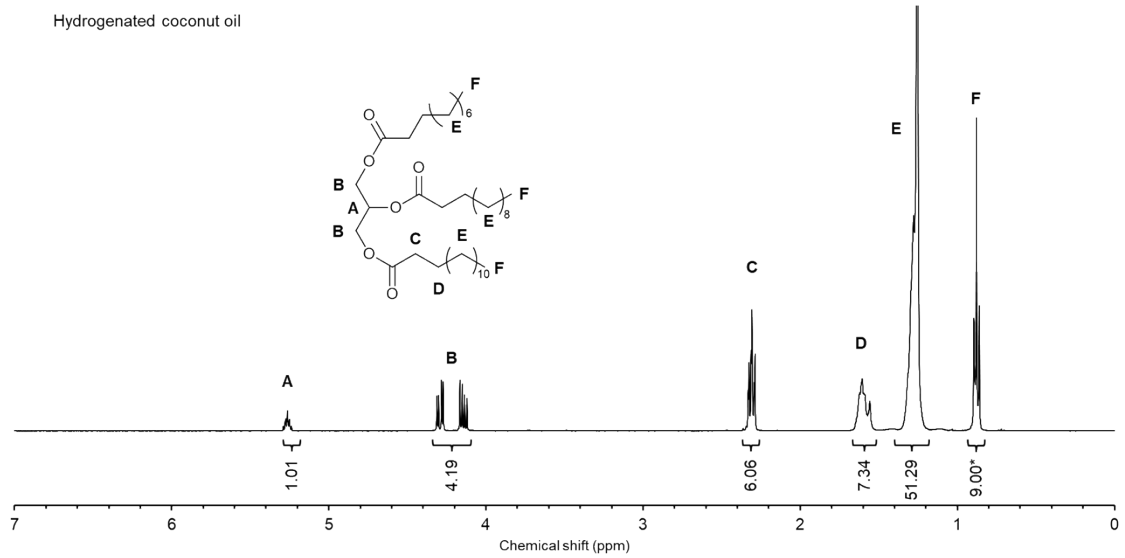

Figure S3. ^{1}H NMR spectrum (400 MHz, $CDCl_3$, 25 °C) of hydrogenated coconut oil. Peaks have been assigned to the target structure and integrals (referenced against the CH_3 signal at 0.88 ppm) are displayed.
^{1}H NMR (400 MHz; $CDCl_3$) δ_H (ppm): 5.26 (1H, m, -O-CH_2-C**H**O-CH_2-O-), 4.22 (4H, m, -O-C**H**$_2$-CHO-C**H**$_2$-O-), 2.33 (6H, t, -OCO-C**H**$_2$-), 1.59 (6H, m, -OCO-CH_2C**H**$_2$-), 1.27 (51H, m, -(C**H**$_2$)$_n$-), 0.88 (6H, t, -C**H**$_3$).

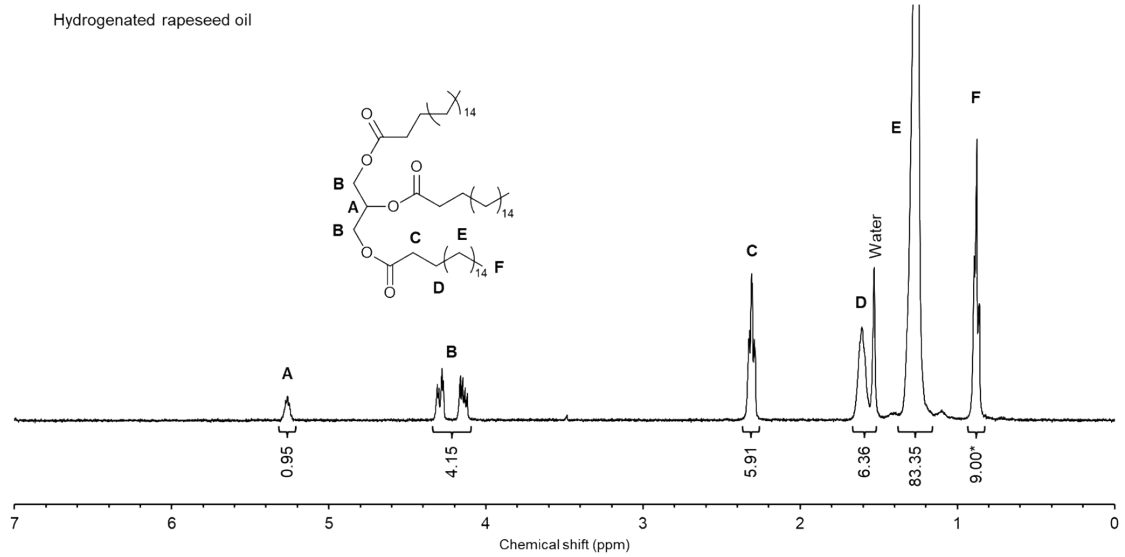

Figure S4. ^{1}H NMR spectrum (400 MHz, $CDCl_3$, 25 °C) of hydrogenated rapeseed oil. Peaks have been assigned to the target structure and integrals (referenced against the CH_3 signal at 0.88 ppm) are displayed.
^{1}H NMR (400 MHz; $CDCl_3$) δ_H (ppm): 5.27 (1H, m, -O-CH_2-C**H**O-CH_2-O-), 4.22 (4H, m, -O-C**H**$_2$-CHO-C**H**$_2$-O-), 2.31 (6H, t, -OCO-C**H**$_2$-), 1.61 (6H, m, -OCO-CH_2C**H**$_2$-), 1.26 (84H, m, -(C**H**$_2$)$_n$-), 0.88 (6H, t, -C**H**$_3$).

Table S1. Fatty acid distributions of each of the feedstock oils used in this study. HO-Sun and hydrogenated coconut oil data obtained from the supplier certificate of analysis. Olive oil and hydrogenated rapeseed oil data informed by literature data [1] and ^{1}H NMR analysis.

	Molar percentage (%)			
Fatty acid (Carbons:alkenes)	**HO-sun oil**	**Olive oil**	**Hydrogenated coconut oil**	**Hydrogenated rapeseed oil**
8:0	0.00	0	6.5	0
10:0	0.00	0	6.0	0
12:0	0.01	0	46.5	0
14:0	0.05	0	18.0	0
16:0	4.63	11	9.5	4
16:1	0.18	0	0	0
18:0	3.01	5	12.0	94
18:1	82.40	75	<2	0
18:2	7.62	8	<1	0
18:3	0.07	1	0	0
20:0	0.28	0	0	2
Saturated (%)	9.3	16	>97	100
Mono-unsaturated (%)	83.0	75	<2	0
Poly-unsaturated (%)	7.7	9	<1	0
Number average chain length	18	18	13	18

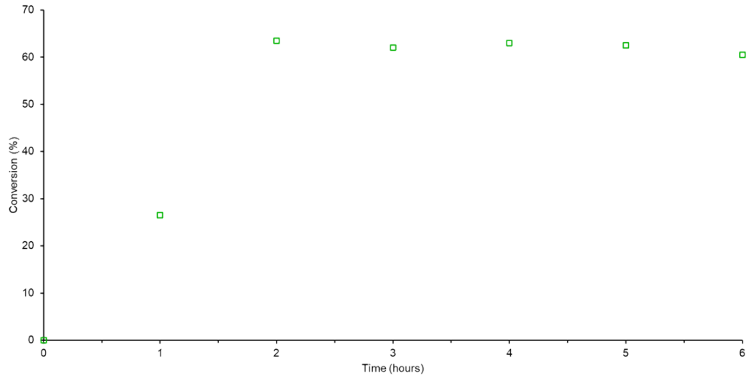

Figure S5. Data from kinetics experiments for the transesterification of commercial extra virgin olive oil with HEAA. Conversion of glyceride bound FAs to POBMs vs time is plotted for a reaction at 30 °C.

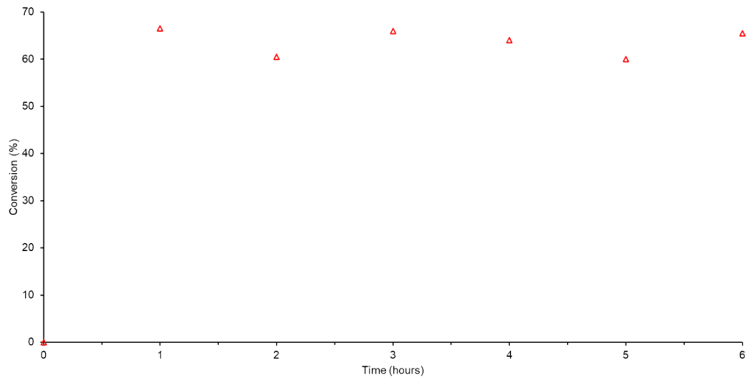

Figure S6. Data from kinetics experiments for the transesterification of hydrogenated coconut oil with HEAA. Conversion of glyceride bound FAs to POBMs vs time is plotted for a reaction at 50 °C.

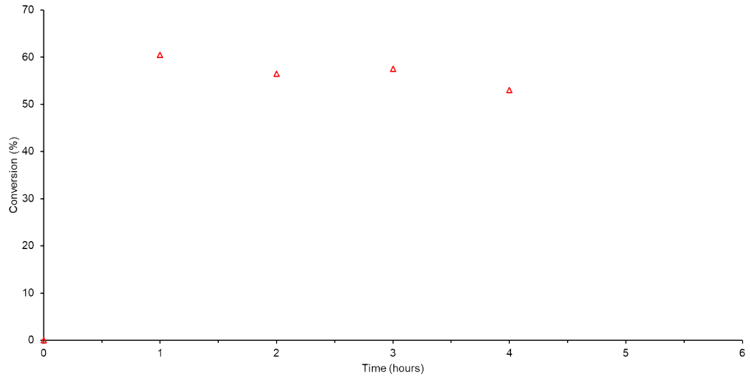

Figure S7. Data from kinetics experiments for the transesterification of hydrogenated rapeseed oil with HEAA. Conversion of glyceride bound FAs to POBMs vs time is plotted for a reaction at 50 °C.

Transesterification side reaction studies

To determine the possibility of side reactions independent of the plant oil in the monomer synthesis, reactions were conducted using a variety of monomeric substituents in otherwise identical stoichiometry to the original synthesis. HEAA (secondary acrylamide with a primary alcohol) was tested along with NIPAM (secondary acrylamide), DMAA (tertiary acrylamide) and HEA (acrylate with a primary alcohol). DMSO was also added as an internal ^{1}H NMR reference.

NIPAM was selected in order to compare another secondary acrylamide without any additional nucleophilic functional groups, and DMA was chosen to assess a tertiary acrylamide. HEMA was chosen in order to evaluate the conjugate addition of alkoxide groups without the possibility of the aza-Michael addition reaction. ^{1}H NMR was used to evaluate vinyl group reaction using DMSO as an internal reference, and SEC analysis was conducted to assess any changes in molecular weight. Results of these experiments can be seen in Table S1.

Table S2. Initial and final M_n values determined by GPC ($CDCl_3$, PS standards), conversion (%) and general observations from the reaction of acrylamide/acrylate monomers in THF with NaOH at 50 °C.

Monomer	Initial $M_{n\ GPC}$	Final $M_{n\ GPC}$	NMR Conversion (%)	Observations
DMA	350	700	44	Tacky solid product, colourless to brown
NIPAM	350	1,300	1*	Tacky solid product, colourless to brown
HEAA	300	650	58	Tacky solid product, colourless to pink
HEMA	300	200	10	No state/ colour change

M_n values were observed to increase post reaction for every monomer, except HEMA which in fact showed a decrease (potentially due to hydrolysis). This implies the formation of polymeric products. Conversions by NMR were substantial for both DMA and HEAA, with a small conversion noted for HEMA, indicating that the increases in M_n are due to reaction of the vinyl groups. Resonances appearing around 2.45 and 1.6 ppm were noted for both the final products of the reactions of HEAA and DMA, which correspond well with acrylamide backbone peaks in the literature and were also observed in the spectrum of the brine washed monomers.[2,3] The low conversion of NIPAM may be due to insolubility of the product species at the experiment temperature as opposed to a lack of reaction (as the largest M_n increase was observed for this monomer). p(NIPAM) is known to exhibit an LCST of around 32 °C, hence any reaction products may have been soluble in the GPC (run at 40 °C) but not in NMR (25 °C). Work by Gur'eva et al. noted that a monomer similar to HEAA, N-hydroxymethyl acrylamide, is relatively unstable and prone to forming N,N-methylenebisacrylamide even after short periods of storage.[3] Work by Lentz et al. performing their own investigation into the stability of HEAA did not find that conditions of THF, 60 °C and an enzymatic catalyst were sufficient to cause a reaction[4] so therefore it is more likely that any reaction here is due to the NaOH. As DMA, a tertiary amide, reacted similarly to HEAA and NIPAM reaction via the amide NH may not be responsible for all of the side reactions occurring in this system. Though the exact nature of any reaction has not been determined, it is abundantly clear from these experiments some reactions independent of the oil feedstock are taking place in the transesterification system presented here.

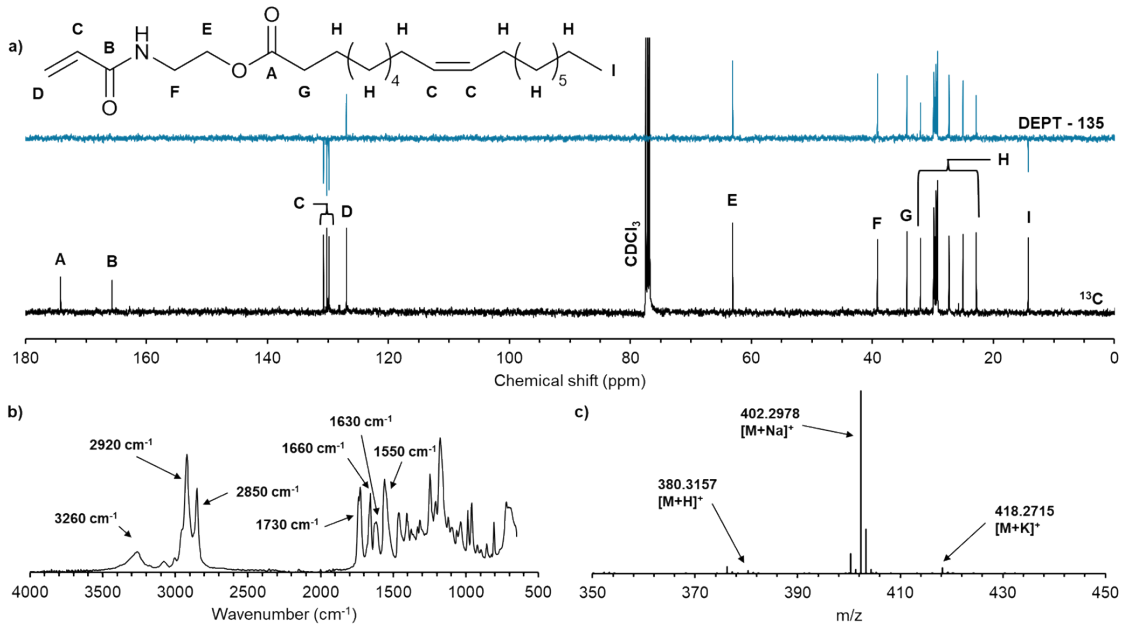

Figure S8. Characterisation of the column purified HOSM. a) ^{13}C NMR and DEPT-135 spectra (100 MHz, $CDCl_3$, 25 °C). Peaks for the column purified sample have been assigned to the target structure. b) FTIR absorbance spectra with major peaks labelled. c) LC-MS ESI spectrum displaying H^+, Na^+ and K^+ adducts of the oleic acid pendant HOSM molecule.

Table S3. Evaluation of LC-MS ESI adduct peaks corresponding to the target HOSM.

Peak m/z	Molecular formula	Theoretical mass	Peak adduct	Predicted adduct m/z	Mass error (ppm)
380.3157	$C_{23}H_{41}NO_3$	379.31	$[M + H]^+$	380.3159	-0.526
402.2978	$C_{23}H_{41}NO_3$	379.31	$[M + Na]^+$	402.2979	-0.249
418.2715	$C_{23}H_{41}NO_3$	379.31	$[M + K]^+$	418.2718	-0.717

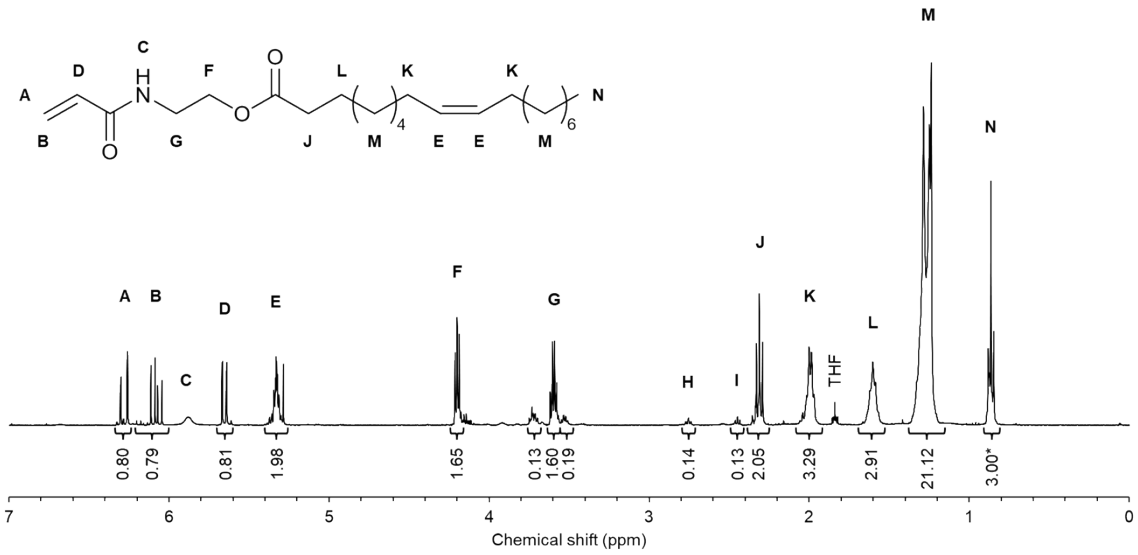

Figure S9. ^{1}H NMR spectra (400 MHz, $CDCl_3$, 25 °C) of brine washed OVM. Peaks have been assigned to the target structure and integrals (referenced against the CH_3 signal at 0.86 ppm) are displayed.

^{1}H NMR (400 MHz; $CDCl_3$) δ_H (ppm): 6.30 (1H, dd, vinyl C**H**$_2$=CH-), 6.11 (1H, dd, vinyl C**H**$_2$=CH-), 5.89 (1H, br s, -N**H**-), 5.65 (1H, dd, vinyl CH_2=C**H**-), 5.35 (2H, m, -CH_2C**H**=C**H**CH_2-, mono-unsaturated FA), 4.19 (2H, t, -NH-CH_2C**H**$_2$-O-), 3.60 (2H, q, -NH-C**H**$_2$$CH_2$-O-), 2.77 (t, =HC-C**H**$_2$-CH=, poly-unsaturated FA), 2.32 (2H, t, -OCO-C**H**$_2$-), 2.02 (4H, m, -C**H**$_2$-CH=CH-C**H**$_2$-, mono-unsaturated FA), 1.64 (2H, m, -OCO-CH_2C**H**$_2$-), 1.27 (20H, m, -(C**H**$_2$)$_n$-), 0.86 (3H, t, -C**H**$_3$).

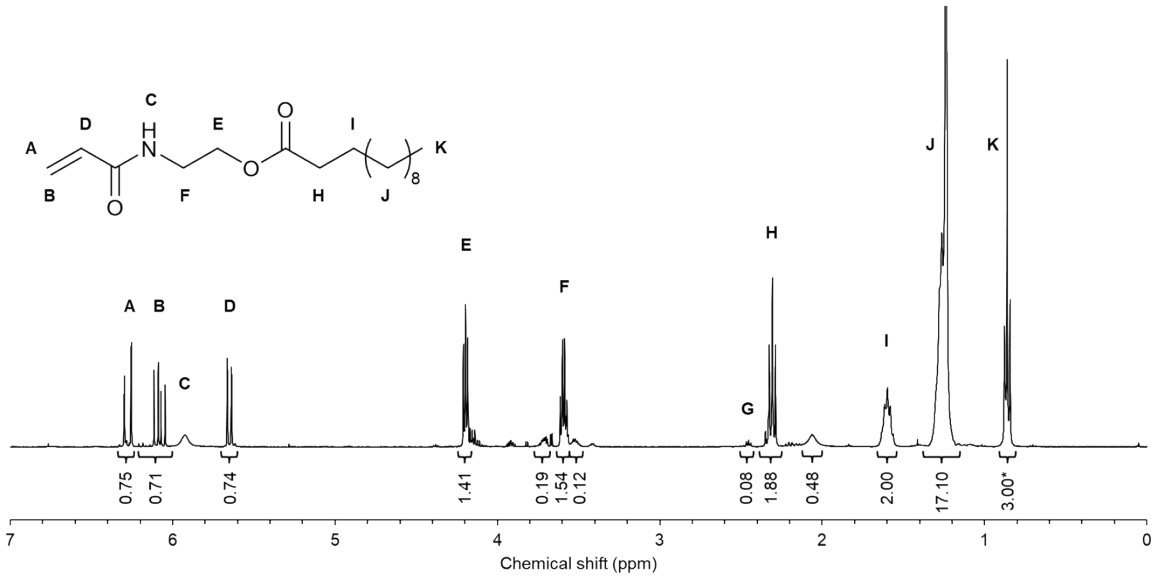

Figure S10. ^{1}H NMR spectra (400 MHz, $CDCl_3$, 25 °C) of brine washed HCM. Peaks have been assigned to the target structure and integrals (referenced against the CH_3 signal at 0.87 ppm) are displayed.

^{1}H NMR (400 MHz; $CDCl_3$) δ_H (ppm): 6.28 (1H, dd, vinyl C**H**$_2$=CH-), 6.10 (1H, dd, vinyl C**H**$_2$=CH-), 5.93 (1H, br s, -N**H**-), 5.65 (1H, dd, vinyl CH_2=C**H**-), 4.21 (2H, t, -NH-CH_2C**H**$_2$-O-), 3.60 (2H, q, -NH-C**H**$_2$$CH_2$-O-), 2.34 (2H, t, -OCO-C**H**$_2$-), 1.60 (2H, m, -OCO-CH_2C**H**$_2$-), 1.26 (17H, m, -(C**H**$_2$)$_n$-), 0.87 (3H, t, -C**H**$_3$).

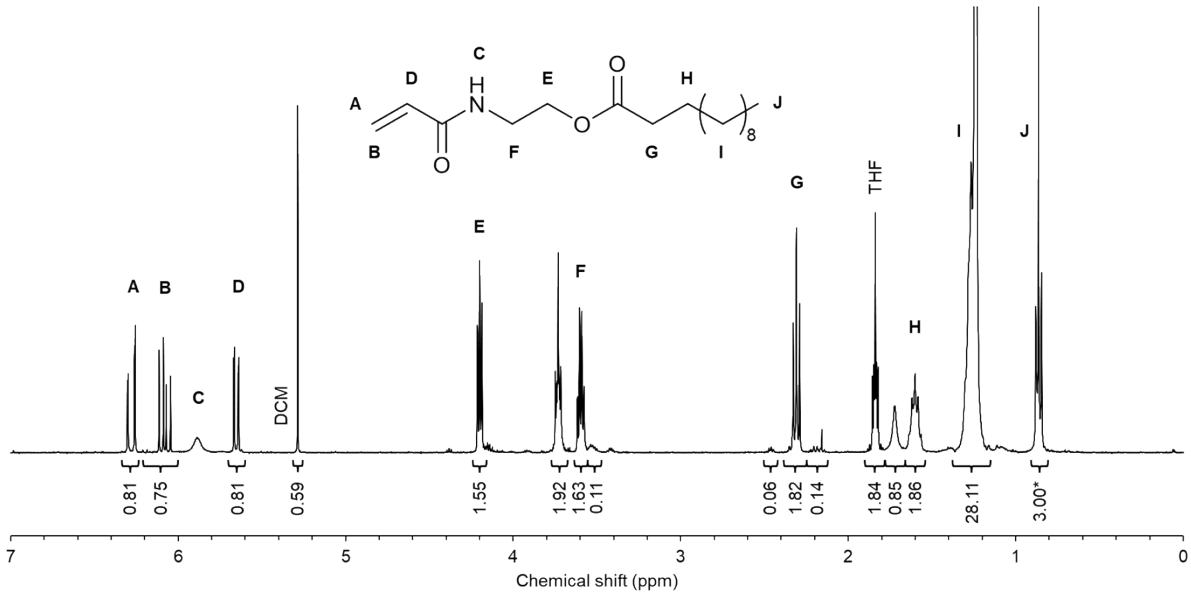

Figure S11. ^{1}H NMR spectra (400 MHz, $CDCl_3$, 25 °C) of brine washed HRM. Peaks have been assigned to the target structure and integrals (referenced against the CH_3 signal at 0.87 ppm) are displayed.

^{1}H NMR (400 MHz; $CDCl_3$) δ_H (ppm): 6.27 (1H, dd, vinyl C**H**$_2$=CH-), 6.09 (1H, dd, vinyl C**H**$_2$=CH-), 5.90 (1H, br s, -N**H**-), 5.66 (1H, dd, vinyl CH_2=C**H**-), 4.20 (2H, t, -NH-CH_2C**H**$_2$-O-), 3.61 (2H, q, -NH-C**H**$_2$$CH_2$-O-), 2.33 (2H, t, -OCO-C**H**$_2$-), 1.60 (2H, m, -OCO-CH_2C**H**$_2$-), 1.23 (28H, m, -(C**H**$_2$)$_n$-), 0.87 (3H, t, -C**H**$_3$).

Table S4. Yield, purity and melting points for monomers synthesised via base catalysed transesterification based on different plant oils and worked up using the brine washing method.

Monomer	POBM yield (%)	POBM purity (mol%) $_{NMR}$	Mpt range (°C) $_{DSC}$
HOSM	56	71	-13.3 - 22.4
OVM	66	72	-17.7 – 19.9
HCM	50	70	3.9 – 39.6
HRM	49	79	69.4 – 76.1

Table S5. Conversion, M_n, *Đ* and thermal degradation data from the analysis of p(POBM)s synthesised by free radical polymerisation (AIBN, toluene, 70 °C, $[M]_0/[I]_0$ = 13).

Polymer	Conversion (%)	$M_{n\ GPC}$ (g mol^{-1})	*Đ*	Onset of thermal degradation (°C)
p(HOSM)	99	25,000	1.76	261
p(OVM)	98	20,400	1.84	260
p(HCM)	99	45,400	2.33	253
p(HRM)	99	47,700	2.52	263

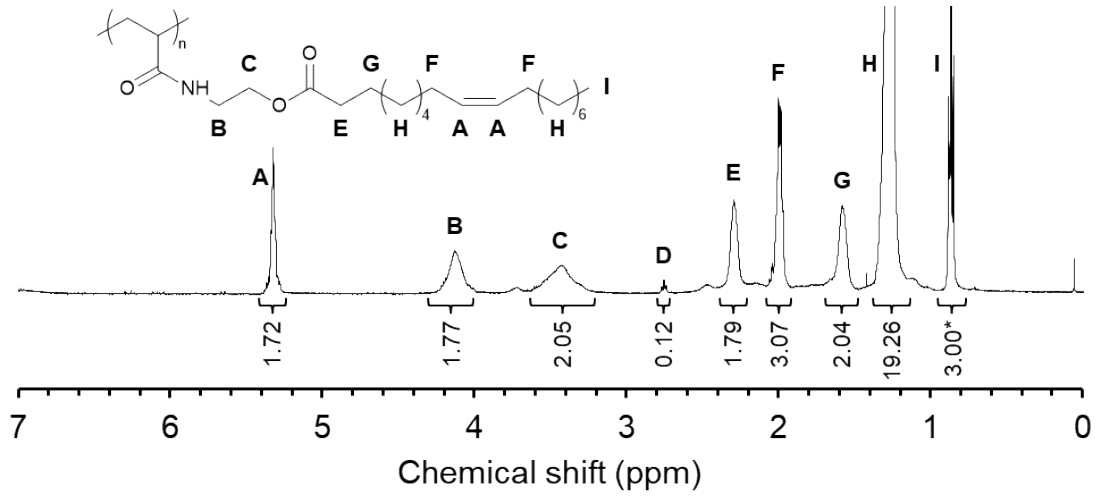

Figure S12. ^{1}H NMR spectra (400 MHz, $CDCl_3$, 25 °C) of p(HOSM) after precipitation in methanol/diethyl ether with peaks assigned to the target structure. Polymer backbone peaks are shallow and broad and overlap with peaks across the region of 0.75-2.75 ppm.

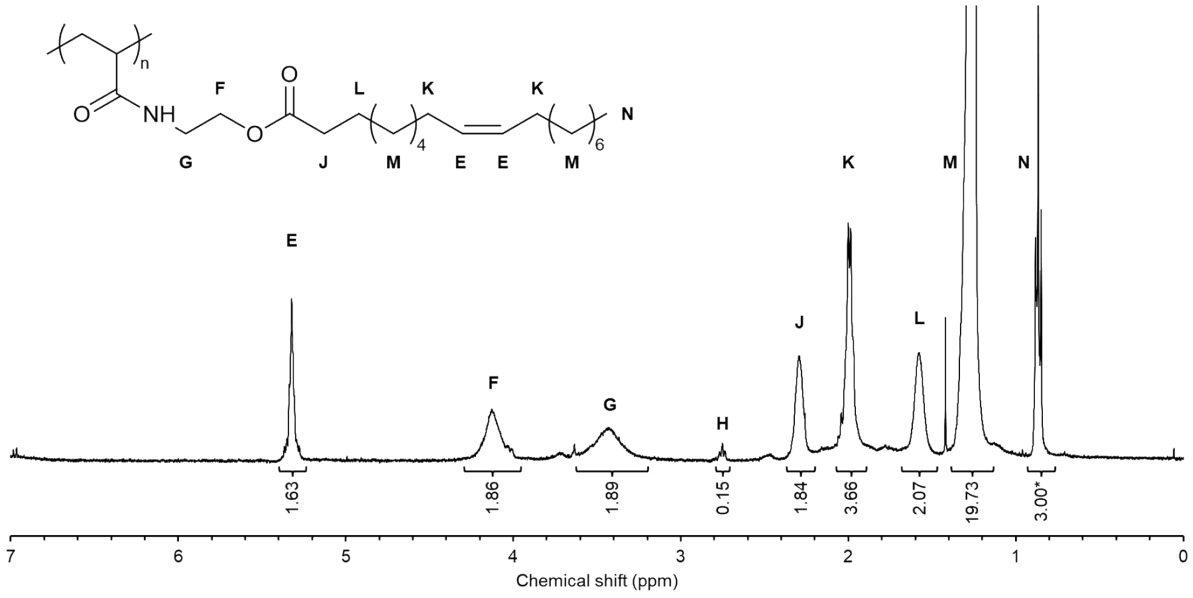

Figure S13. ^{1}H NMR spectra (400 MHz, $CDCl_3$, 25 °C) of p(OVM) after precipitation in methanol/diethyl ether with peaks assigned to the target structure. Polymer backbone peaks are shallow and broad and overlap with peaks across the region of 0.75-2.75 ppm.

^{1}H NMR (400 MHz; $CDCl_3$) δ_H (ppm): 6.98 (1H, br s, -N**H**-), 5.36 (2H, m, -CH_2C**H**=C**H**CH_2-, mono-unsaturated FA), 4.17 (2H, br, -NH-CH_2C**H**$_2$-O-), 3.76 (br, co-monomer unit), 3.55 (2H, br, -NH-C**H**$_2$$CH_2$-O-), 2.76 (t, =HC-C**H**$_2$-CH=, poly-unsaturated FA), 2.51 (br, co-monomer unit), 2.31 (2H, br, -OCO-C**H**$_2$-), 2.04 (4H, br, -C**H**$_2$-CH=CH-C**H**$_2$-, mono-unsaturated FA), 1.59 (2H, br, -OCO-CH_2C**H**$_2$-), 1.28 (20H, m, -(C**H**$_2$)$_n$-), 0.88 (3H, t, -C**H**$_3$), 2.75-0.75 (3H, br, p(OVM) backbone).

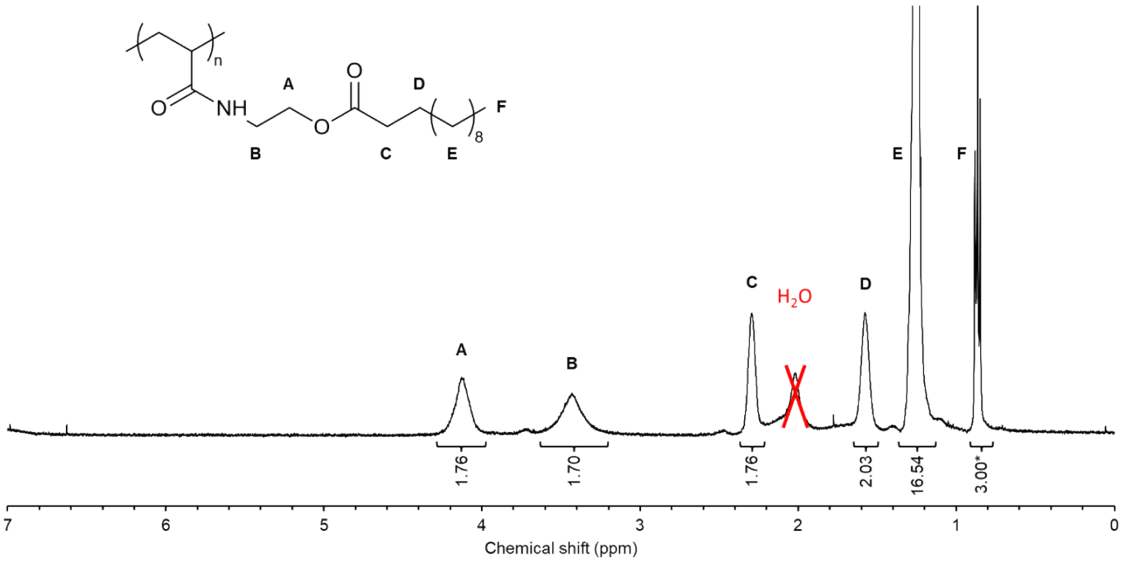

Figure S14. ^{1}H NMR spectra (400 MHz, $CDCl_3$, 25 °C) of p(HCM) after precipitation in methanol/diethyl ether with peaks assigned to the target structure. Polymer backbone peaks are shallow and broad and overlap with peaks across the region of 0.75-2.75 ppm.

^{1}H NMR (400 MHz; $CDCl_3$) δ_H (ppm): 7.00 (1H, br s, -N**H**-), 4.14 (2H, br, -NH-CH_2C**H**$_2$-O-), 3.74 (br, co-monomer unit), 3.48 (2H, br, -NH-C**H**$_2$$CH_2$-O-), 2.50 (br, co-monomer unit), 2.31 (2H, br, -OCO-C**H**$_2$-), 1.59 (2H, br, -OCO-CH_2C**H**$_2$-), 1.25 (17H, m, -(C**H**$_2$)$_n$-), 0.88 (3H, t, -C**H**$_3$), 2.75-0.75 (3H, br, p(HCM) backbone).

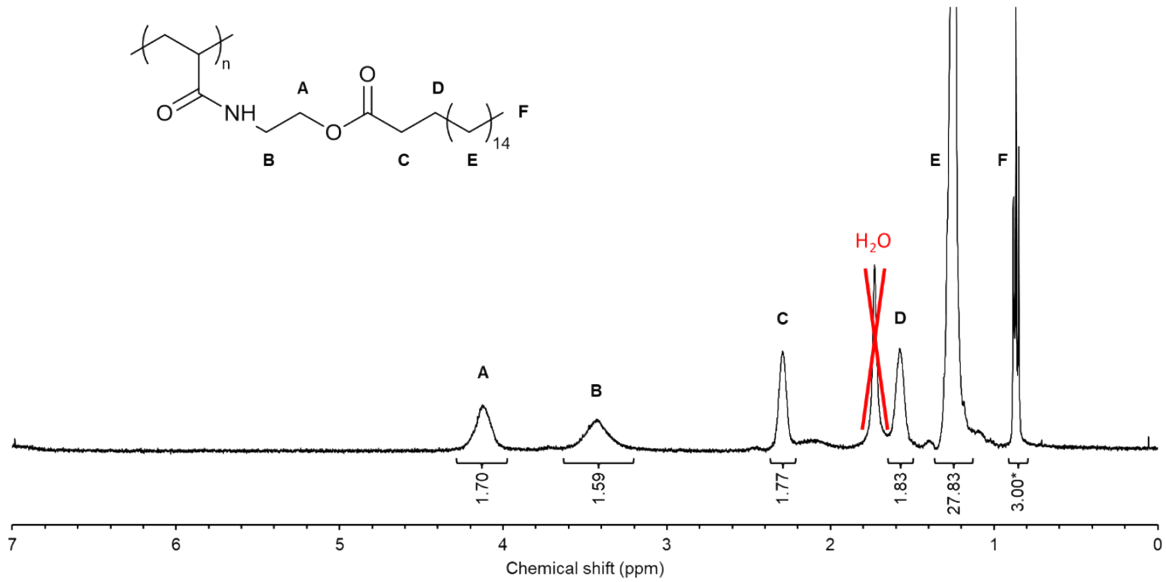

Figure S15. ^{1}H NMR spectra (400 MHz, $CDCl_3$, 25 °C) of p(HRM) after precipitation in methanol/diethyl ether with peaks assigned to the target structure. Polymer backbone peaks are shallow and broad and overlap with peaks across the region of 0.75-2.75 ppm.

^{1}H NMR (400 MHz; $CDCl_3$) δ_H (ppm): 6.98 (1H, br s, -N**H**-), 4.20 (2H, br, -NH-CH_2C**H**$_2$-O-), 3.73 (br, co-monomer unit), 3.41 (2H, br, -NH-C**H**$_2$$CH_2$-O-), 2.47 (br, co-monomer unit), 2.29 (2H, br, -OCO-C**H**$_2$-), 1.58 (2H, br, -OCO-CH_2C**H**$_2$-), 1.23 (28H, m, -(C**H**$_2$)$_n$-), 0.89 (3H, t, -C**H**$_3$), 2.75-0.75 (3H, br, p(HCM) backbone).

Table S6. Results of the initial RAFT agent screening (OVM, AIBN, toluene, 70 °C, 24 h, $[M]_0:[CTA]_0:[I]_0$ = 50:1:0.2, 25 wt% solids content).

CTA	Conversion (%)	$M_{n\ th}$	$M_{n\ GPC}$	$Đ_{GPC}$
DDMAT (2-(Dodecylthiocarbonothioylthio)-2-methylpropionic acid)	87	16,900	7,700	1.33
CPDT (2-Cyano-2-propyl dodecyl trithiocarbonate)	47	9,300	6,400	1.21
CECPA (4-((((2- Carboxyethyl)thio)carbonothioyl)thio)-4-cyanopentanoic acid)	58	11,300	6,700	3.36
CDTPA (4-Cyano-4- [(dodecylsulfanylthiocarbonyl)sulfanyl]pentanoic acid)	81	15,800	10,400	1.24

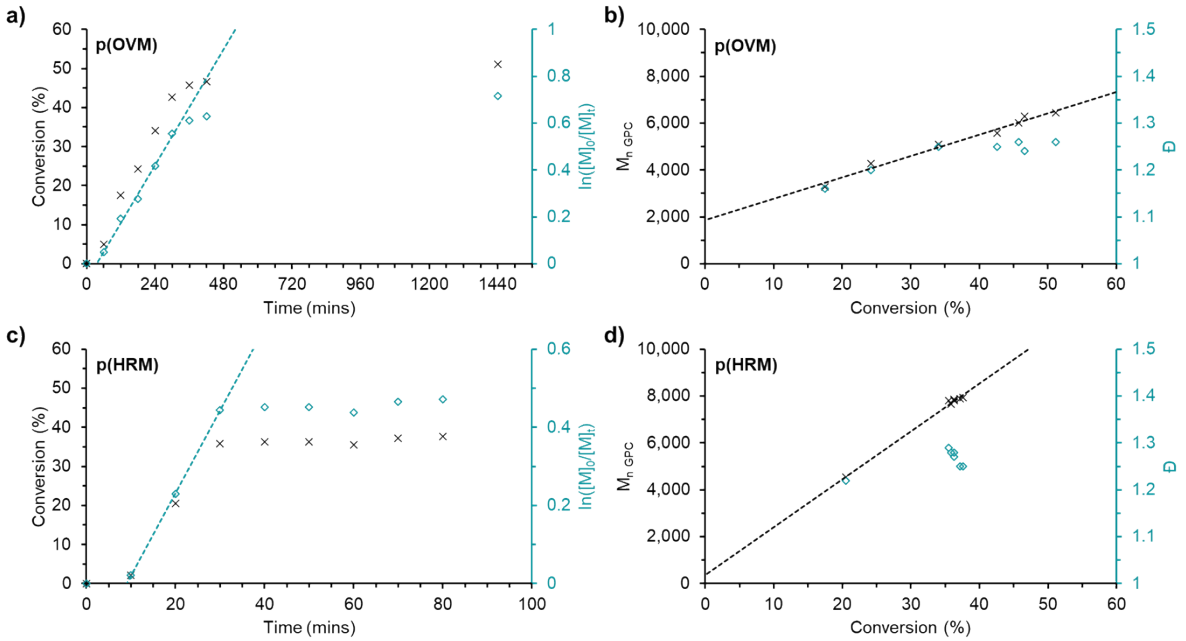

Figure S16. Plots from kinetics experiments on the RAFT polymerisation of brine washed POBMs at a target DP of 50 (AIBN, toluene, 70 °C). a) Conversion (%) and $\ln([M]_0/[M]_t)$ vs time (mins) plots of p(OVM). b) M_n and Đ vs conversion (%) plots of p(OVM). c) Conversion (%) and $\ln([M]_0/[M]_t)$ vs time (mins) plots of p(HRM). d) M_n and Đ vs conversion (%) plots of p(HRM).

Table S7. Summary of key data from the kinetics experiments shown on the RAFT polymerisation of brine washed OVM and HRM at a target DP of 50 (AIBN, toluene, 70 °C). $K_{p\ app}$ calculated from the gradient of the linear region of the $\ln([M]_0/[M]_t)$ plot.

Polymer	Max conversion (%)	$M_{n\ th}$ (g mol^{-1})	$M_{n\ GPC}$ (g mol^{-1})	Đ	$k_{p\ app}$ ($hours^{-1}$)
p(OVM)	51	10,000	6,400	1.26	0.13
p(HRM)	38	7,600	7,900	1.25	1.27

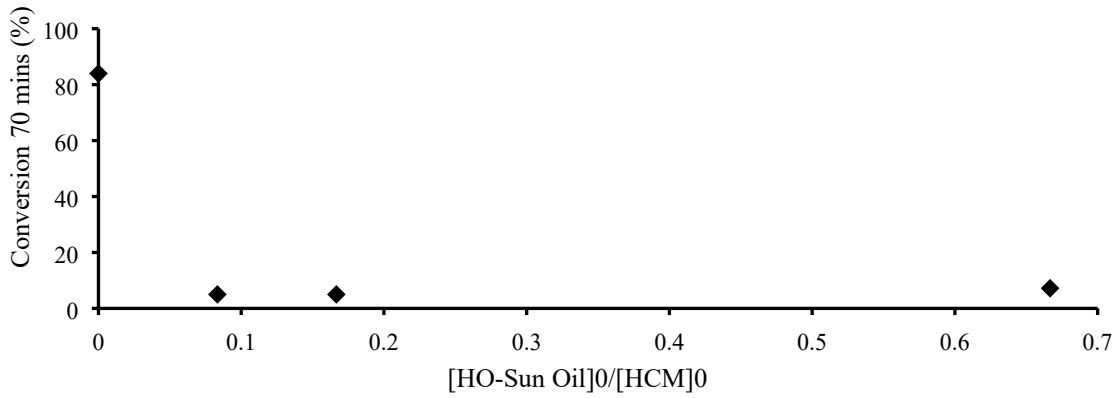

Figure S17. Conversion (%) of HCM after RAFT polymerisation (toluene at 70 °C) in solution with several concentrations of HO-sun oil after 70 minutes. The conversion is seen to drop sharply after the addition of even a very low concentration of HO-sun oil.

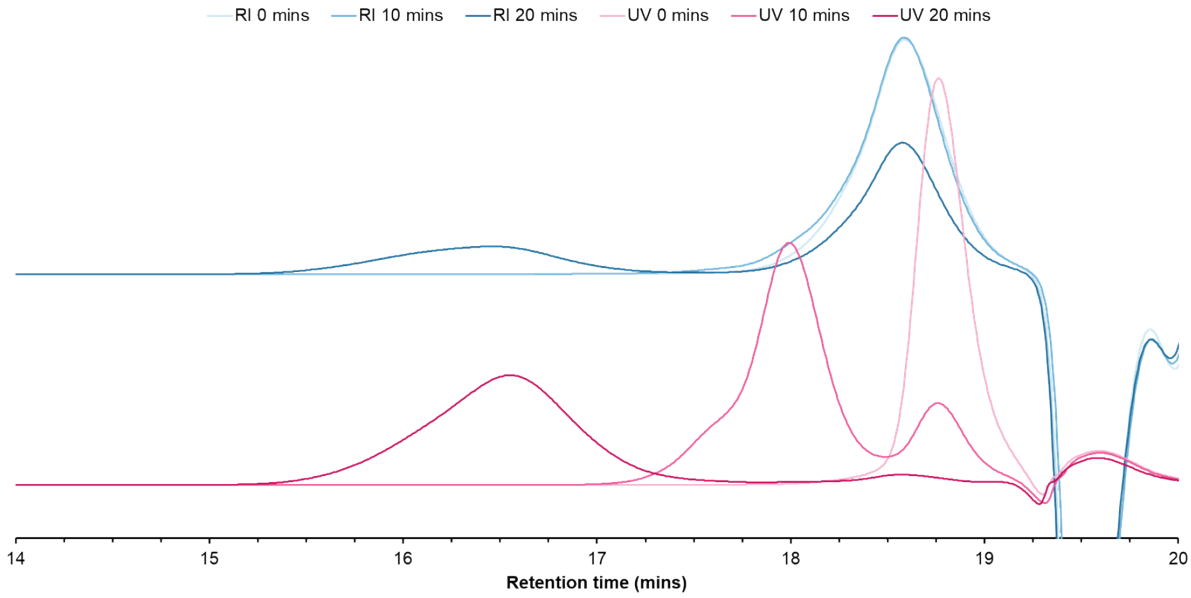

Figure S18. GPC chromatograms (THF) of kinetics samples of the RAFT polymerisation of HCM showing evidence of RAFT pre-equilibrium species formation. The peak visible in the UV trace at a retention time of 18 mins is not visible in the RI trace in the 10 minute sample, however both signals overlap in the sample from the next time point after further propogation of the polymer chain.

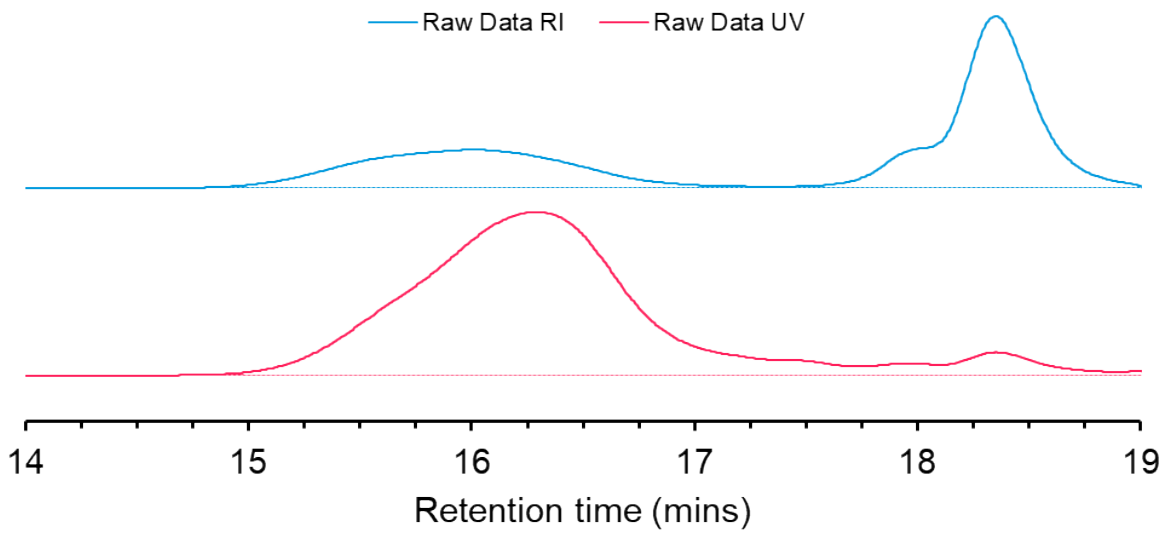

Figure S19. RAFT end group fidelity of p(HCM) is demonstrated using GPC (THF) via the simultaneous detection of polymer chains by the RI and UV detectors.

Table S8. Results of the second RAFT agent screening (brine washed HOSM, AIBN, toluene, 70 °C, 24 h, $[M]_0$:$[CTA]_0$:$[I]_0$ = 50:1:0.2, 25 wt% solids content).

CTA	Conversion (%)	$M_{n\ th}$	$M_{n\ GPC}$	$Đ_{GPC}$
DDMAT (2-(Dodecylthiocarbonothioylthio)-2-methylpropionic acid)	50	9,900	7,200	1.26
DDTPA (2-(Dodecylthiocarbonothioylthio)propionic acid)	66	12,900	10,500	1.22
CDT (Cyanomethyl dodecyl trithiocarbonate)	69	13,400	10,700	1.22
Pyrazole (cyanomethyl (3,5-Dimethyl-1H-pyrazole)-carbodithioate)	74	14,200	12,200	1.25

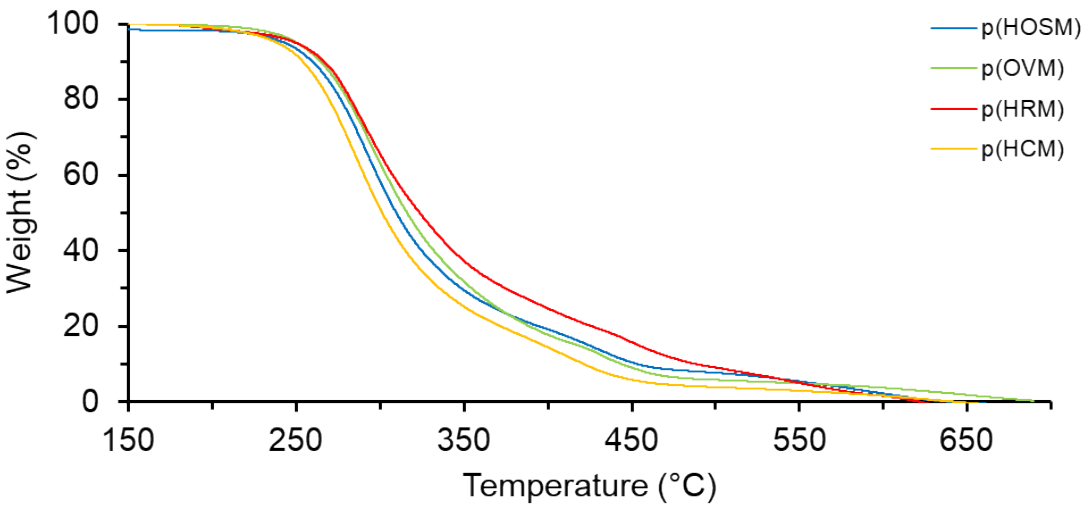

Figure S20. Weight loss (%) vs temperature (°C) plots from TGA of all p(POBM)s synthesised by free radical polymerisation showing comparable degradation behaviour.

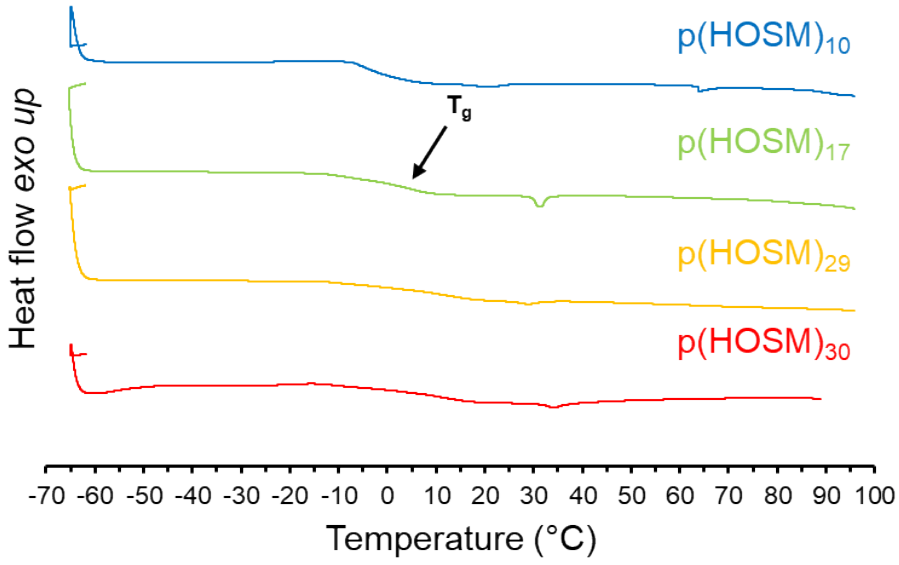

Figure S21. Heat flow vs temperature (°C) plots from DSC (10 °C min^{-1}) of p(HOSM) samples with DP_{NMR} from 10 to 30. Amorphous behaviour was observed for all samples and the value of T_g was observed to increase with M_n as expected from the Flory-Fox relationship.

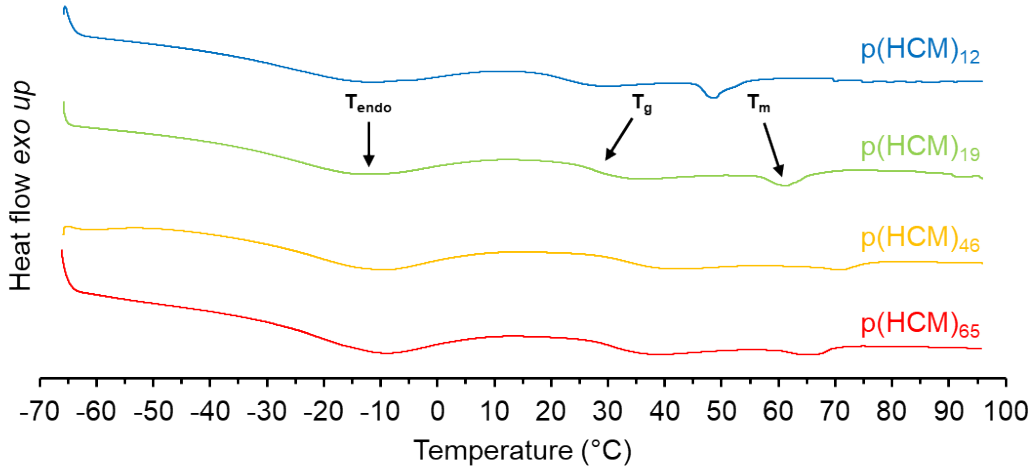

Figure S22. Heat flow vs temperature (°C) plots from DSC (10 °C min^{-1}) of p(HCM) samples with DP_{NMR} from 12 to 65. Semi-crystalline behaviour was observed for all samples, and the values of T_g and T_m were observed to increase with M_n for the DP 12, 19 and 46 as expected from the Flory-Fox relationship. A slight decrease in T_g and T_m was observed for the DP 65 sample from the DP 46, the cause of which remains unclear (potential causes could include plasticisation from trace impurities, branching).

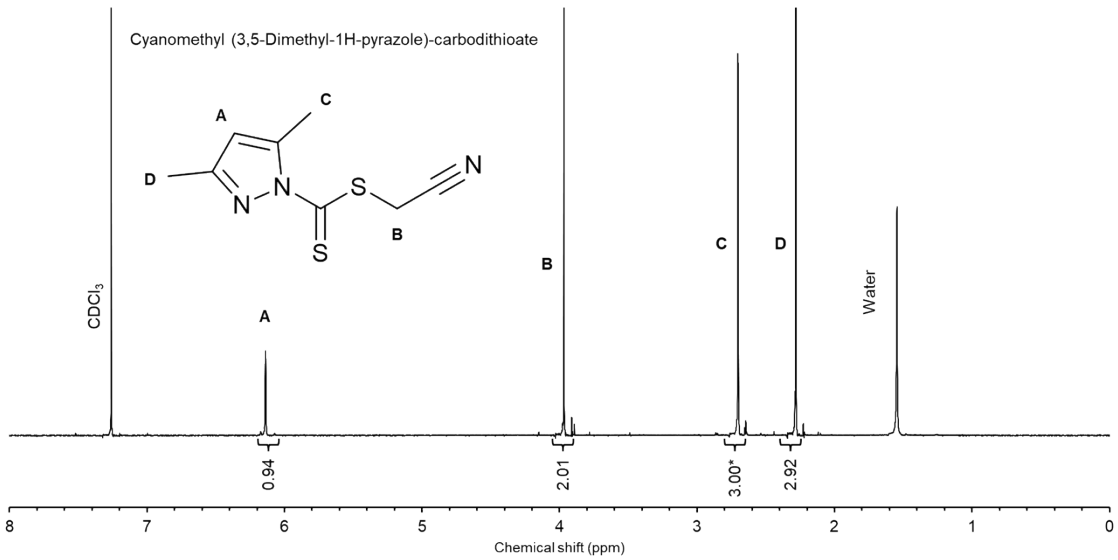

Figure S23. ^{1}H NMR spectra (400 MHz, $CDCl_3$, 25 °C) of (3,5-dimethyl-1H-pyrazole)-carbodithioate (py-CTA) with peaks assigned to the chemical structure. Peak integrals were referenced against the -C**H**$_3$ peak at 2.67 ppm.

^{1}H NMR (400 MHz; $CDCl_3$) δ_H (ppm): 6.16 (1H, s, Ar**H**), 3.93 (2H, s, -S-C**H**$_2$-CN), 2.67 (3H, s, -CH=C(C**H**$_3$)-N-), 2.25 (3H, s, -CH-C(C**H**$_3$)=N-).

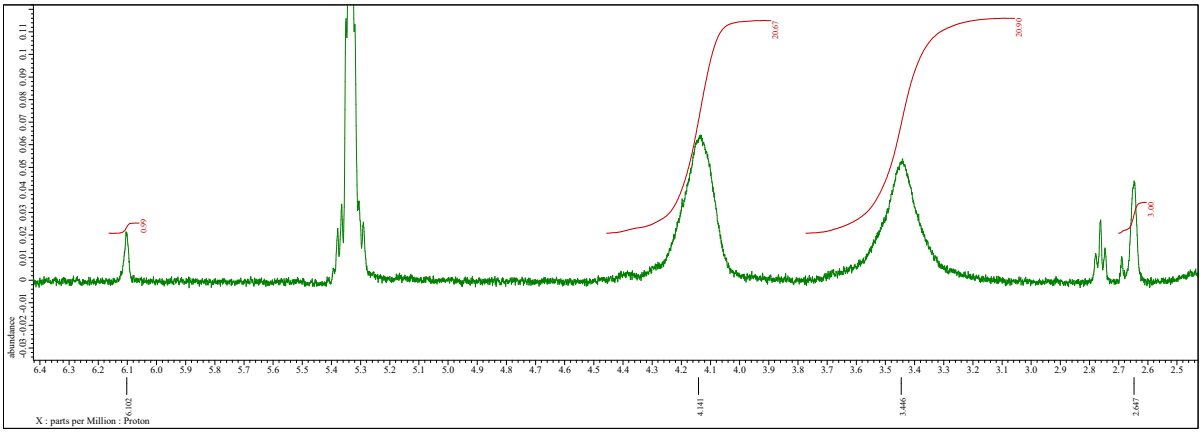

Figure S24. ^{1}H NMR spectra (400 MHz, $CDCl_3$, 25 °C) of $p(HOSM)_{10}$ (pyrazole, AIBN, toluene, 70 °C) after precipitation in methanol/diethyl ether with peaks assigned to the target structure.

End group analysis of $p(HOSM)_{10}$ from RAFT polymerisation with the pyrazole CTA was performed by comparing the ratio of the integrals of the CTA's -C**H**$_3$ and -Ar**H** peaks at 2.67 and 6.16 ppm with those of the -O-C**H**$_2$-C**H**$_2$-NH- peaks of the p(HOSM) repeat unit.

References

1 R. C. Zambiazi, R. Przybylski, M. W. Zambiazi and C. B. Mendonca, *Boletim do Centro de Pesquisa de Processamento de Alimentos*, 2007, **25**, 111–120.

2 Y. Sun, L. Fu, M. Olszewski, K. Matyjaszewski, Y. Sun, L. Fu, M. Olszewski and K. Matyjaszewski, *Macromol Rapid Commun*, 2019, **40**, 1800877.

3 L. L. Gur'eva, A. I. Tkachuk, Y. I. Estrin, B. A. Komarov, E. A. Dzhavadyan, G. A. Estrina, L. M. Bogdanova, N. F. Surkov and B. A. Rozenberg, *Polymer Science - Series A*, 2008, **50**, 283–290.

4 J. C. Lentz, R. Cavanagh, C. Moloney, B. Falcone Pin, K. Kortsen, H. R. Fowler, P. L. Jacob, E. Krumins, C. Clark, F. Machado, N. Breitkreuz, B. Cale, A. R. Goddard, J. D. Hirst, V. Taresco and S. M. Howdle, *Polym Chem*, 2022, **13**, 6032–6045.